Oriented Growth of Calcite Controlled by Self-Assembled Monolayers of Functionalized Alkanethiols Supported on Gold and Silver

Joanna Aizenberg,*,† Andrew J. Black,‡ and George M. Whitesides*,‡

Contribution from Bell Laboratories, Lucent Technologies, 600 Mountain Avenue, Murray Hill, New Jersey 07974, and Department of Chemistry and Chemical Biology, Harvard University, 12 Oxford Street, Cambridge, Massachusetts 02138

Received December 9, 1998

Abstract: This paper describes the oriented nucleation of calcite controlled by self-assembled monolayers (SAMs) of ω-terminated alkanethiols ($HS(CH_2)_nX$) supported on metal films. The effect of the chemistry and geometry of the organic surfaces was surveyed by using different functional groups (X = CO_2^-, SO_3^-, PO_3^{2-}, OH, $N(CH_3)_3^+$, CH_3) and different supporting metals (Au and Ag). Optical microscopy, SEM with image analysis, and XRD were employed to characterize density and orientation of the crystals. Compared to the control surfaces of bare metal films, SAMs terminated in CO_2^-, SO_3^-, PO_3^{2-}, and OH groups were more active in inducing nucleation, whereas SAMs terminated in $N(CH_3)_3^+$ and CH_3 inhibited nucleation. The crystallographic orientations of the crystals were distinct and highly homogeneous for each surface, but different on different surfaces. SAMs of CO_2^-/Au, CO_2^-/Ag, OH/Au, OH/Ag, SO_3^-/Au, and SO_3^-/Ag induced the face-selective nucleation of calcite from the (015), (012), (104), (103), (1 0 12), and (107) crystallographic planes, respectively. SAMs of PO_3^{2-}/Au and PO_3^{2-}/Ag were specific for a family of planes that form an angle of 24° and 40° with the *c*-axis, respectively. The high degree of orientational uniformity of the overgrown crystals (97−100% oriented crystals for well-ordered SAMs) and the decrease of uniformity as the defect density in the SAMs increased imply that nucleation takes place from the oriented, homogeneous SAM and that the specific interfacial structure is controlling orientation of crystal growth. The possible correlation between the differences in the structure of SAMs supported on Au and Ag and the orientation of the incipient crystals is discussed. Varying the geometry, chemistry, and pattern of the functional groups on SAMs provides, therefore, a tool for a fine-tuning of the orientation of crystal growth and for the formation of high-resolution patterns of oriented crystals.

Introduction

This paper describes the face-selective nucleation of crystals of calcium carbonate on self-assembled monolayers (SAMs) of ω-terminated alkanethiols ($HS(CH_2)_nX$) supported on thin, evaporated films of Au and Ag as substrates. The ability of structured organic surfaces to control nucleation of crystal growth in biological and synthetic environments[1−9] has prompted a number of model studies on oriented crystallization of inorganic and organic materials using Langmuir monolayers,[10−14] biological macromolecules[4,15] and functionalized polymer surfaces.[16−18] Although these organic surfaces are able to induce oriented growth of crystals, the specificity of face-selective nucleation has generally not been high, and the processes could not be easily controlled because the structures of these organic surfaces were neither homogeneous nor well-defined.

In contrast, alkanethiols on metal substrates form monolayers with high order.[19] The structures of these SAMs have been extensively characterized.[20−24] The alkyl chains adopt an

† Bell Laboratories, Lucent Technologies.
‡ Harvard University.

(1) Lowenstam, H. A.; Weiner, S. *On Biomineralization*; Oxford University Press: Oxford, 1989.
(2) Mann, S.; Webb, J.; Williams, R. J. P., Eds. *Biomineralization: Chemical and Biochemical Perspectives*; VCH Publishers: Weinheim, 1989.
(3) Alper, M.; Calvert, P. D.; Frankel, R.; Rieke, P. C.; Tirrell, D. A. *Materials Synthesis Based on Biological Processes*; Materials Research Society: Pittsburgh, PA, 1991.
(4) Addadi, L.; Weiner, S. *Proc. Natl. Acad. Sci. U.S.A.* **1985**, *82*, 4110−4113.
(5) Mann, S. *Nature* **1993**, *365*, 499−505.
(6) Bunker, B. C.; Rieke, P. C.; Tarasevich, B. J.; Campbell, A. A.; Fryxell, G. E.; Graff, G. L.; Song, L.; Liu, J.; Virden, J. W.; McVay, G. L. *Science* **1994**, *264*, 48−55.
(7) Firouzi, A.; Kumar, D.; Bull, L. M.; Besier, T.; Sieger, P.; Huo, Q.; Walker, S. A.; Zasadzinski, J. A.; Glinka, C.; Nicol, J.; Margolese, D.; Stucky, G. D.; Chmelka, B. F. *Science* **1995**, *267*, 1138−1143.
(8) Mann, S.; Ozin, G. A. *Nature* **1996**, *382*, 313−318.
(9) Stupp, S. I.; Braun, P. V. *Science* **1997**, *277*, 1242−1248.
(10) Landau, E. M.; Levanon, M.; Leiserowitz, L.; Lahav, M.; Sagiv, J. *Nature* **1985**, *318*, 353−356.
(11) Landau, E. M.; Wolf, S. G.; Levanon, M.; Leiserowitz, L.; Lahav, M.; Sagiv, J. *J. Am. Chem. Soc.* **1989**, *111*, 1436−1445.
(12) Zhao, X. K.; McCormick, L. D. *Appl. Phys. Lett.* **1992**, *61*, 849−851.
(13) Heywood, B. R.; Mann, S. *Adv. Mater.* **1994**, *6*, 9−20.
(14) Frostman, L. M.; Ward, M. D. *Langmuir* **1997**, *13*, 330−337.
(15) Addadi, L.; Moradian, J.; Shay, E.; Maroudas, N. G.; Weiner, S. *Proc. Natl. Acad. Sci. U.S.A.* **1987**, *84*, 2732−2736.
(16) Feng, S.; Bein, T. *Science* **1994**, *265*, 1839−1841.
(17) Berman, A.; Ahn, D. J.; Lio, A.; Salmeron, M.; Reichert, A.; Charych, D. *Science* **1995**, *269*, 515−518.
(18) Aksay, I. A.; Trau, M.; Manne, S.; Honma, I.; Yao, N.; Zhou, L.; Fenter, P.; Eisenberger, P. M.; Gruner, S. M. *Science* **1996**, *273*, 892−898.
(19) Ulman, A. *An Introduction to Ultrathin Organic Films: From Langmuir−Blodgett to Self-Assembly*; Academic Press: San Diego, CA, 1991.
(20) Laibinis, P. E.; Whitesides, G. M. *J. Am. Chem. Soc.* **1992**, *114*, 1990−1995.

10.1021/ja984254k CCC: $18.00
Published on Web 04/24/1999

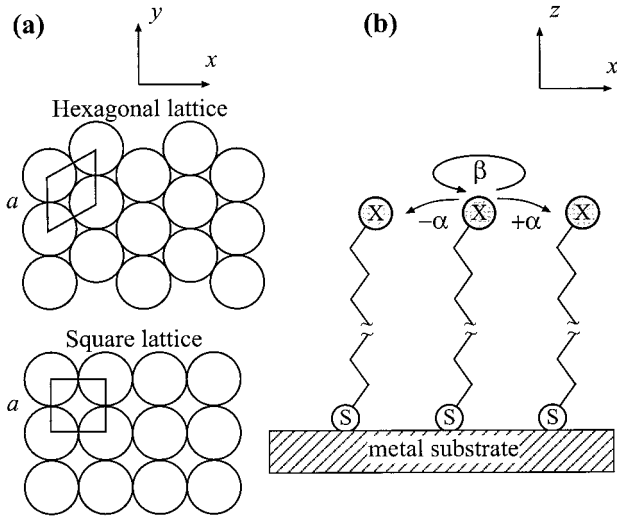

Figure 1. Schematic illustration of the structure of monolayers of ω-terminated *n*-alkanethiols on a metal substrate. (a) View down the surface normal, showing the symmetry of the sulfur sublattice and interchain distance *a*. (b) View parallel to the surface, showing the cant angle α and the twist angle β. The initial orientation of the all-trans hydrocarbon chain is perpendicular to the surface and with the plane of the carbon chain parallel to the *XZ* plane. Positive values of α correspond to tilts in the direction of the S−C bond.

extended, largely trans conformation. Figure 1 summarizes parameters used in describing the geometry of SAMs—the symmetry of the structure, the distance between the chains (*a*), the angle and direction of the tilt of the chain ($\pm\alpha$), and the twist angle around the axis of the chain (β). The ease of preparation and extensive structural background of SAMs of alkanethiols on metals makes them an attractive candidate for an organic surface to control oriented growth of crystals.[25−27]

We chose the crystallization of calcium carbonate on monolayers of $HS(CH_2)_nX$ ($X = CO_2^-$, SO_3^-, PO_3^{2-}, OH, $N(CH_3)_3^+$, CH_3) as a model system for three reasons: (i) calcite [a stable polymorph of calcium carbonate, space group $R\bar{3}c$, $a = 4.99$ Å, $c = 17.06$ Å (Figure 2)] has a simple structure, and its crystallization is relatively easy to perform;[28] (ii) precipitation of calcium carbonate has been studied extensively by others, and there is a broad background of relevant information for this system;[15,17,26,28−34] and (iii) the crystallographically oriented

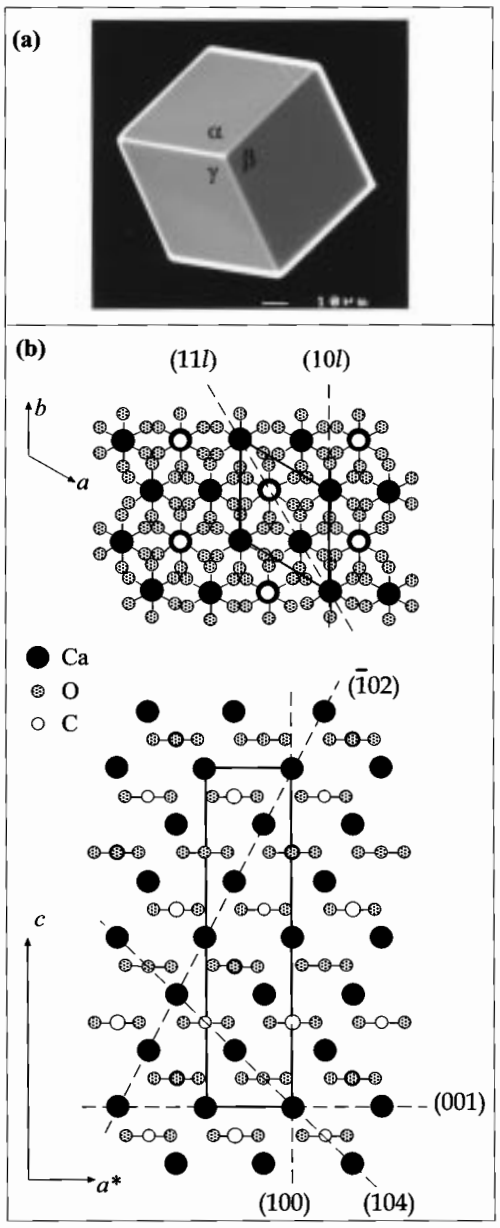

Figure 2. (a) Scanning electron micrograph of the regular {104} calcite rhombohedron. The angles α, β, γ unequivocally define the crystallographic orientation of the crystal. (b) Calcite structure viewed down the *c* axis (top) and down the *b* axis (bottom). The directions of the crystallographic axes, the unit cell, and important crystallographic planes are indicated.

growth of calcite is common in biological environments,[1,2] and is usually controlled by acidic macromolecules, conceivably by virtue of a match between the structures of the organic surface and that of a particular crystal plane.[4,15,31,35−37] We hoped, therefore, that structurally different SAMs might induce the formation of crystals in different crystallographic directions. Indeed, CO_2^--, SO_3^--, and OH-terminated SAMs induced highly oriented growth of calcite, each in a specific crystallographic direction. The PO_3^{2-} -terminated SAMs induced limited crystallographic specificity; that is, crystals nucleated from different planes, but from planes that form the same angle with the *c*

(21) Nuzzo, R. G.; Dubois, L. H.; Allara, D. L. *J. Am. Chem. Soc.* **1990**, *112*, 558−569.
(22) Laibinis, P. E.; Whitesides, G. M.; Allara, D. L.; Tao, Y.-T.; Parikh, A. N.; Nuzzo, R. G. *J. Am. Chem. Soc.* **1991**, *113*, 7152−7167.
(23) Sellers, H.; Ulman, A.; Shnidman, Y.; Eilers, J. E. *J. Am. Chem. Soc.* **1993**, *115*, 9389−9401.
(24) Camillone, N.; Chidsey, C. E. D.; Liu, G.; Scoles, G. *J. Chem. Phys.* **1993**, *98*, 4234−4245.
(25) Rieke, P. C.; Tarasevich, B. J.; Wood, L. L.; Engelhard, M. H.; Baer, D. R.; Fryxell, G. E.; John, C. M.; Laken, D. A.; Jaehnig, M. C. *Langmuir* **1994**, *10*, 619−622.
(26) Archibald, D. D.; Qadri, S. B.; Gaber, B. P. *Langmuir* **1996**, *12*, 538−546.
(27) Gupta, V. K.; Abbott, N. L. *Science* **1997**, *276*, 1533−1536.
(28) Lippmann, F. *Sedimentary Carbonate Minerals*; Springer-Verlag: Berlin, 1973.
(29) Mann, S.; Heywood, B. R.; Rajam, S.; Birchall, J. D. *Nature* **1988**, *334*, 692−695.
(30) Mann, S.; Heywood, B. R.; Rajam, S.; Walker, J. B. A. *J. Phys. D-Appl. Phys.* **1991**, *24*, 154−164.
(31) Berman, A.; Addadi, L.; Weiner, S. *Nature* **1988**, *331*, 546−548.
(32) Belcher, A. M.; Wu, X. H.; Christensen, R. J.; Hansma, P. K.; Stucky, G. D.; Morse, D. E. *Nature* **1996**, *381*, 56−58.
(33) Falini, G.; Albeck, S.; Weiner, S.; Addadi, L. *Science* **1996**, *271*, 67−69.
(34) Lahiri, J.; Xu, G. F.; Dabbs, D. M.; Yao, N.; Aksay, I. A.; Groves, J. T. *J. Am. Chem. Soc.* **1997**, *119*, 5449−5450.
(35) Albeck, S.; Aizenberg, J.; Addadi, L.; Weiner, S. *J. Am. Chem. Soc.* **1993**, *115*, 11691−11697.
(36) Aizenberg, J.; Albeck, S.; Weiner, S.; Addadi, L. *J. Cryst. Growth* **1994**, *142*, 156−164.
(37) Aizenberg, J.; Hanson, J.; Ilan, M.; Koetzle, T. F.; Addadi, L.; Weiner, S. *FASEB J.* **1995**, *9*, 262−268.

Table 1. Nomenclature for the ω-Substituted Alkanethiols Used for the Formation of SAMs

	substrate	
thiol	Au	Ag
$HS(CH_2)_{15}CO_2^-$	CO_2^-/Au	CO_2^-/Ag
$HS(CH_2)_{11}OH$	OH/Au	OH/Ag
$HS(CH_2)_{11}SO_3^-$	SO_3^-/Au	SO_3^-/Ag
$HS(CH_2)_{11}PO_3^{2-}$	PO_3^{2-}/Au	PO_3^{2-}/Ag
$HS(CH_2)_{15}CH_3$	CH_3/Au	CH_3/Ag
$HS(CH_2)_{11}N(CH_3)_3^+$	$N(CH_3)_3^+$/Au	$N(CH_3)_3^+$/Ag
	bare Au	bare Ag

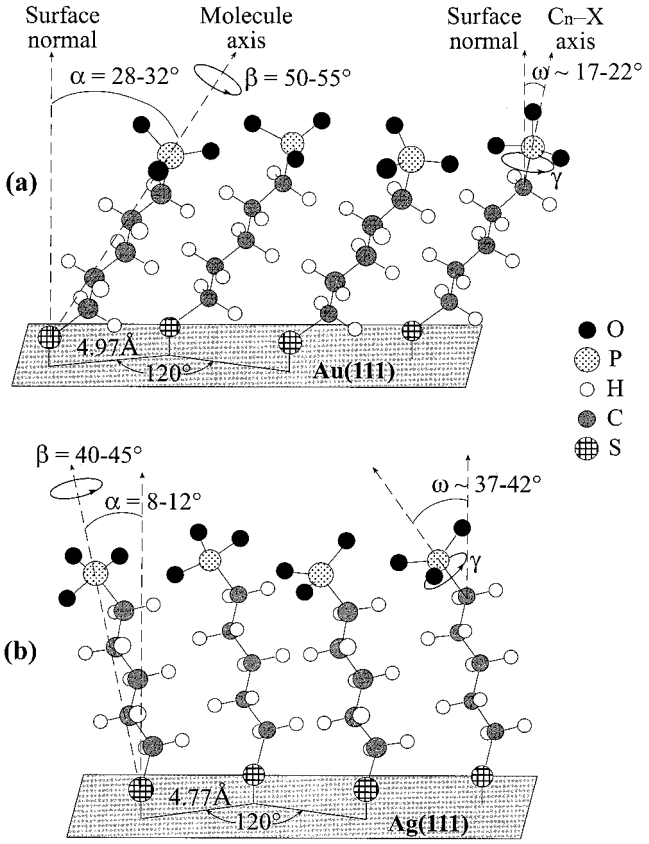

Figure 3. Geometry of SAMs of $HS(CH_2)_nX$ supported on Au(111) (a) and Ag(111) (b). The example of a PO_3^{2-}-terminated SAM is shown.

crystallographic axis. The $N(CH_3)_3^+$- and CH_3-terminated SAMs inhibited crystallization. These results demonstrate that SAMs of ω-terminated alkanethiols on metals can be used to control the orientation of crystal growth.

Results and Discussion

Self-Assembled Monolayers. We formed SAMs of alkanethiols terminated in different functional groups ($HS(CH_2)_nX$) on films of gold and silver. Table 1 lists the nomenclature used in the text to define the different SAMs.

Figure 3 shows the simplified geometry of SAMs on Au and Ag.[19−22] Alkanethiols terminated in different functional groups self-assemble on Au(111) in a hexagonal array with similar structural parameters (Figure 3a): $a = 4.97$ Å, $\alpha = 28-32°$, and $\beta = 50-55°$.[21] The structural parameters for SAMs on Ag(111) are different from those for SAMs on Au(111) (Figure 3b): X-terminated alkanethiols self-assemble on Ag(111) in a hexagonal overlayer with $a = 4.77$ Å, $\alpha = 8-12°$, and $\beta = 42-45°$.[22] There is, however, ambiguity in the precise orientation of the headgroups and uncertainty in the order of the outer part of the SAM, because the terminal groups are, in principle, free to rotate around the C_n-X bond (angle γ in Figure 3), and are capable of interacting with each other. This freedom results in considerable disordering of the interface.[21,38−41]

X-ray studies of the structure of monolayers[42−45] have shown that the presence of bound counterions, such as Cd^{2+} and Ca^{2+}, increases the order of the surface for carboxylic acid terminated Langmuir monolayers and SAMs, due to the formation of a counterion overlayer. For example, adsorption of Ca^{2+} ions at pH 6−8 at the surface of the SAM of $HS(CH_2)_{15}CO_2H$ supported on Au (111)[45] (our experimental conditions) has been claimed to result in a counterion overlayer composed of one Ca^{2+}, one OH^-, and one H_2O with the ratio of Ca^{2+} to CO_2^- of about 1:1, and a specific, preferred orientation of the carboxylate groups. We expected that ordering of the surface in the presence of counterions would favor oriented crystallization.

Crystallization of Calcium Carbonate. To study the preorganization of the surface in the presence of counterions, and to demonstrate its importance for controlled, face-selective nucleation, we grew calcite crystals on SAMs by mixing together equal volumes of 0.1 M aqueous solutions of $NaHCO_3$ and $CaCl_2$ in different sequences. For SAMs of CO_2^-/Au, CO_2^-/Ag, SO_3^-/Au, and SO_3^-/Ag, we observed highly oriented, surface-induced nucleation when the SAMs were exposed to the $CaCl_2$ solution first and the $NaHCO_3$ solution was added thereafter. There was no preferred orientation when the SAMs were first exposed to the $NaHCO_3$ solution and the $CaCl_2$ solution was added subsequently, presumably as a result of nonspecific precipitation rather than surface-induced nucleation. For SAMs of OH/Au and OH/Ag, the selectivity of oriented growth was reduced noticeably in experiments in which the SAMs were first exposed to the $NaHCO_3$ solution relative to those in which they were first exposed to the $CaCl_2$ solution.

Table 2 shows the general results of the crystallization experiments on SAMs with different terminal groups supported on Au and Ag, as studied by optical microscopy. Four random regions for each surface were analyzed. The areas of the analyzed regions were 1×1 mm^2 for OH-, CH_3-, and $N(CH_3)^+$-terminated SAMs and bare metals and 0.25×0.25 mm^2 for CO_2^--, PO_3^{2-}-, and SO_3^- -terminated SAMs. Crystallization of calcium carbonate on control surfaces of bare metal films resulted in the formation of a mixture of two polymorphs—calcite (~85%) and vaterite (~15%). Acidic SAMs were more active than bare metal films in inducing nucleation, and produced 6−50 times higher densities of crystals (Table 2). The crystals were calcite rhombohedra expressing stable cleavage {104} faces (Figure 2).[28] The density of nucleation on hydroxy-terminated SAMs was slightly (~1.5 times) higher than that on the corresponding bare substrates (Table 2). The crystals were exclusively calcite. The methyl-terminated SAMs were one-

(38) Larsen, N. B.; Biebuyck, H.; Delamarche, E.; Michel, B. *J. Am. Chem. Soc.* **1997**, *119*, 3017−3026.
(39) Camillone, N.; Chidsey, C. E. D.; Eisenberger, P.; Fenter, P.; Li, J.; Liang, K. S.; Liu, G. Y.; Scoles, G. *J. Chem. Phys.* **1993**, *99*, 744−747.
(40) Smith, E. L.; Alves, C. A.; Anderegg, J. W.; Porter, M. D.; Siperko, L. M. *Langmuir* **1992**, *8*, 2707−2714.
(41) Lee, T. R.; Carey, R. I.; Biebuyck, H. A.; Whitesides, G. M. *Langmuir* **1994**, *10*, 741−749.
(42) Leveiller, F.; Jacquemain, D.; Lahav, M.; Leiserowitz, L.; Deutsch, M.; Kjaer, K.; Alsnielsen, J. *Science* **1991**, *252*, 1532−1536.
(43) Zasadzinski, J. A.; Viswanathan, R.; Madsen, L.; Garnaes, J.; Schwartz, D. K. *Science* **1994**, *263*, 1726−1733.
(44) Böhm, C.; Leveiller, F.; Jacquemain, D.; Mohwald, H.; Kjaer, K.; Alsnielsen, J.; Weissbuch, I.; Leiserowitz, L. *Langmuir* **1994**, *10*, 830−836.
(45) Li, J.; Liang, K. S.; Scoles, G.; Ulman, A. *Langmuir* **1995**, *11*, 4418−4427.

Table 2. Crystallization of Calcium Carbonate on SAMs of Alkanethiols Supported on Gold and Silver Studied by Optical Microscopy

SAM	polymorph: calcite (%)/vaterite (%)	density of nucleation (crystals/mm^2)	size of crystals, (μm)	type of nucleation of calcite
Bare Au	82/18	107 ± 12	28 ± 11	random
Bare Ag	86/14	125 ± 19	26 ± 9	random
CO_2^-/Au	100/0	1980 ± 124	12 ± 5	oriented
CO_2^-/Ag	100/0	6040 ± 236	8 ± 3	oriented
OH/Au	100/0	152 ± 10	27 ± 4	oriented
OH/Ag	100/0	188 ± 11	25 ± 3	oriented
SO_3^-/Au	100/0	3120 ± 183	10 ± 3	oriented
SO_3^-/Ag	100/0	8680 ± 127	6 ± 1	oriented
PO_3^{2-}/Au	99/1	574 ± 38	17 ± 5	random
PO_3^{2-}/Ag	100/0	856 ± 50	14 ± 4	random
CH_3/Au	67/33	47 ± 14	35 ± 12	random
CH_3/Ag	71/29	62 ± 16	32 ± 10	random
$N(CH_3)_3^+$/Au	no crystallization			
$N(CH_3)_3^+$/Ag	no crystallization			

half as active in forming nucleation sites than was a bare substrate, and also induced formation of a mixture of calcite (~70%) and vaterite (~30%) (Table 2). Amine-terminated SAMs totally inhibited crystallization. Even at the optical scale of observation, the crystals grown on CO_2^-/Au, CO_2^-/Ag, OH/Au, OH/Ag, SO_3^-/Au, and SO_3^-/Ag were largely oriented.

Orientation of Calcite Grown on Functionalized SAMs Supported on Au. The predominant crystallographic orientations of the calcite crystals were determined from the XRD profiles and from morphological analysis (see Experimental Section).

Representative XRD spectra are shown in Figure 4. For the quantitative analysis of the orientational uniformity (Table 3), we normalized the measured intensities of peaks in these spectra by standard intensities of peaks for randomly oriented calcite powder (Figure 4, top).[46] The percentage of calcite crystals in different orientations (*hkl*) was estimated using eq 1:

$$\%_{hkl} = 100 \times \frac{I_{hkl}/I^*_{hkl}}{\sum_{hkl}(I_{hkl}/I^*_{hkl})} \qquad (1)$$

The results show that crystals grown on CO_2^-/Au, OH/Au, and SO_3^-/Au have a pronounced orientational uniformity: the predominant nucleating planes (NP_{XRD}) were (015) for CO_2^-/Au (73% for the (0 2 10) reflection), (104) for OH/Au (91% for the (104) reflection), and (1 0 10) for SO_3^-/Au (56% for the (1 0 10) reflection). The observed NP_{XRD} for crystals grown on CH_3/Au, bare Au, and PO_3^{2-}/Au were largely random, but the latter surface showed slight preference for nucleation from the (018), (1 0 10), (1 1 12), and (0 1 14) planes (15−25% each). X-ray analysis is, however, limited to the characterization of crystals that nucleate only from the standard diffraction planes (listed in Figure 4, top, and Table 3, column 1). Crystals nucleated specifically from any other crystallographic plane cannot be detected from the XRD spectra. The qualitative characterization of the predominant nucleating planes is, therefore, approximate, and the percentages of oriented crystals that we report from the X-ray measurements will probably be lower than the actual values in most instances.

The SEM image analysis of crystal morphologies provides a more precise crystallographic characterization of oriented crystals. We visualized the morphological results using the sphere of reflection;[47] every point on this sphere represents a certain crystallographic plane (Figure 5a). According to symmetry considerations, we used one-sixth of the sphere and divided it into about 200 regions, that is, the neighboring regions form an angle of about 6° with each other (Figure 5b). The nucleating planes for each surface type measured by morphological analysis were plotted as circles on the sphere with a 5% gray scale; the intensity of the gray scale of the final circles is

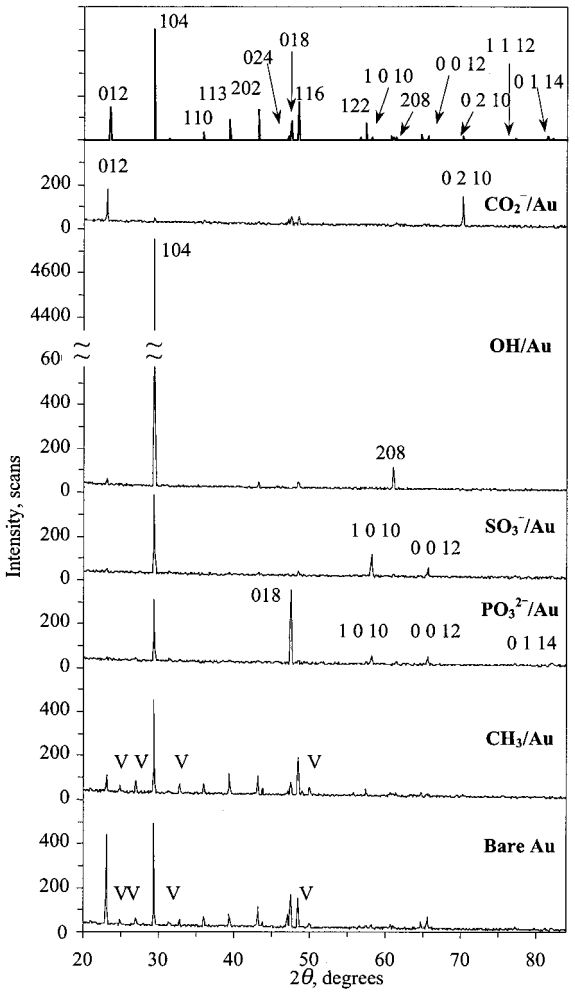

Figure 4. X-ray diffraction data of calcite crystals grown on monolayers of $HS(CH_2)_nX$ supported on gold. Top: A standard diffraction spectrum of the randomly oriented calcite powder.[46] The indices of the crystallographic planes are indicated over the corresponding diffraction lines. Symbol "V" denotes reflections from vaterite.

(46) Joint Committee on Powder Diffraction Standards—International Center for Diffraction Data, Swarthmore, U.K., 1986; File No. 24-27 (Calcite).

(47) Klug, H. P.; Alexander, L. E. *X-ray Diffraction Procedures*; Wiley-Interscience: New York, NY, 1974.

Table 3. Crystallographic Orientation of Calcite Crystals Grown on SAMs Supported on Gold Estimated from XRD Data

		CO_2^-/Au		OH/Au		SO_3^-/Au		PO_3^{2-}/Au		CH_3/Au		bare Au	
h k l	standard int, *I** [a]	*I*[b]	%[c]	*I*[b]	%[c]	*I*[b]	%[c]	*I*[b]	%[c]	*I*[b]	%[c]	*I*[b]	%[c]
0 1 2	29	100	9.5	1	3.1	2	0.4	2	0.3	18	5.0	88	13.6
1 0 4	100	15	0.4	100	**90.8**	100	5.3	84	3.1	100	8.1	100	4.5
1 1 0	7	8	3.1							10	11.5	9	5.7
1 1 3	18					2	0.6	1	0.2	22	9.8	11	2.7
2 0 2	27	5	0.5	1	3.4	2	0.4	2	0.3	20	6.0	19	3.1
0 1 8	17	24	3.9					100	21.4	13	6.2	32	8.4
1 1 6	34	22	1.8	1	2.7	4	0.6	4	0.4	41	9.7	28	3.7
2 1 1	2											2	4.5
1 2 2	15							1	0.2	7	3.8	2	0.6
1 0 10	2					21	**55.6**	11	20.0			3	6.7
2 1 4	3									4	10.7	4	6.0
1 1 9	2	4	5.5					3	5.5	3	12.1		
3 0 0	5									4	6.4	7	6.3
0 0 12	3	3	2.7			9	15.9	10	12.1	3	8.1	11	16.4
0 2 10	3	79	**72.6**							1	2.7		
1 1 12	<1					2	21.2	3	21.9			1	8.9
2 1 10	3												
0 1 14	<1							2	14.6			1	8.9

[a] JCPDS data[46] showing the intensities of peaks in the XRD profile for randomly oriented calcite powder. [b] Measured intensity of peaks in XRD profiles of calcite crystals grown on different surfaces. [c] Percentage of crystals in different orientations estimated using eq 1.

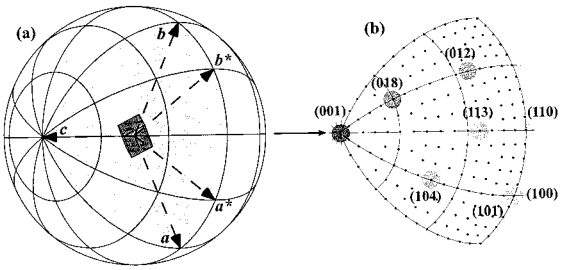

Figure 5. (a) Sphere of reflection for calcite. (b) Part of the sphere used to present morphological analysis of crystal orientations (see text for description).

proportional to the number of crystals in the corresponding orientation. The example shown in Figure 5b would correspond to the morphological measurements of a set of 40 crystals in which one crystal nucleated from the (101) plane, two from the (110) plane, three from the (100) plane, four from the (113) plane, five from the (104) plane, six from the (012) plane, eight from the (018) plane, and 11 from the (001) plane.

Figure 6 shows the morphological results for the orientations of crystals formed on different SAMs supported on Au. The positions of the average nucleating planes estimated from the morphological analysis (NP_{MA}) are compared to the predominant orientations observed in the corresponding XRD profiles (indicated by arrows). The CO_2^-/Au, OH/Au, and SO_3^-/Au SAMs showed a significant clustering of the data: the NP_{MA} were (015), (104), and (1 0 12), respectively (Figure 6a−c). The distribution of crystals reveals further information: in the case of PO_3^{2-}/Au, the crystals—whose XRD profiles and appearance in SEM failed to show crystallographic specificity—appeared to all nucleate selectively from planes that form the same angle (∼24°) with the *c*-axis (Figure 6d). This angle corresponds well to the angle ω formed by the C_n−P bond in the monolayer with the surface normal (see Figure 3a). The nucleating planes that belong to the same zone observed in our experiments may result from the free rotation of the PO_3 group that plays the role of a surrogate anion for the nucleating crystals. The orientations of calcite crystals were clearly random for CH_3/Au and bare Au (Figure 6e,f).

Figure 7 shows representative scanning electron micrographs (SEMs) of oriented calcite crystals grown on various SAMs supported on Au. The inserts illustrate the computer simulations

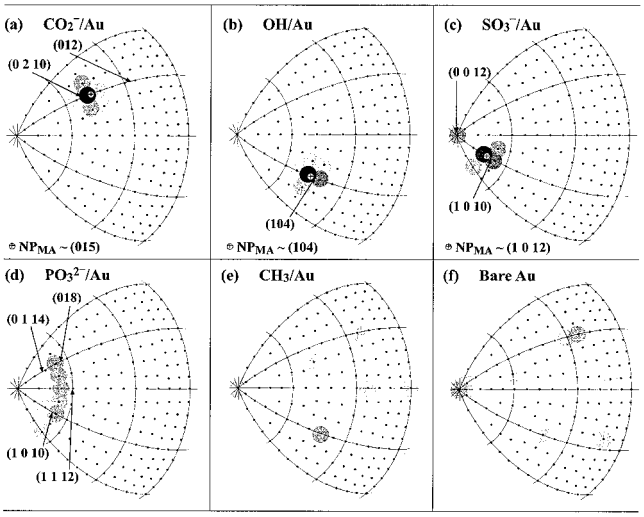

Figure 6. Morphological analysis of orientations of calcite crystals grown on SAMs supported on gold: (a) CO_2^-/Au; (b) OH/Au; (c) SO_3^-/Au; (d) PO_3^{2-}/Au; (e) CH_3/Au; (f) bare Au. The indices of the crystallographic planes are indicated.

of the crystals nucleated from the corresponding NP_{MA} derived from Figure 6; the two correlate well.

Orientation of Calcite Grown on Functionalized SAMs Supported on Ag. The XRD spectra of calcite crystals grown on SAMs supported on Ag are shown in Figure 8. Table 4 presents the estimated percentage of calcite crystals in different orientations. The XRD data confirmed the preliminary optical information on orientational specificity for CO_2^-/Ag and OH/Ag: NP_{XRD} were assigned as the (012) (82% for the (012) reflection) and (104) (81% for the (104) reflection) planes, respectively. For SO_3^-/Ag, an increased intensity (31.7%) was observed for the reflections from the (104) and (1 0 10) planes. The observed NP_{XRD} for crystals grown on CH_3/Ag, bare Ag, and PO_3^{2-}/Ag were largely random, but the latter surface showed slight preference for the nucleation of calcite from the (104), (119), (0 1 5), and (2 1 10) planes (15−25%).

Figure 9 illustrates the more precise morphological characterization of oriented crystals using the sphere of reflections. The CO_2^-/Ag, OH/Ag, and SO_3^-/Ag SAMs showed a significant clustering of the data: NP_{MA} were (012), (103), and (107),

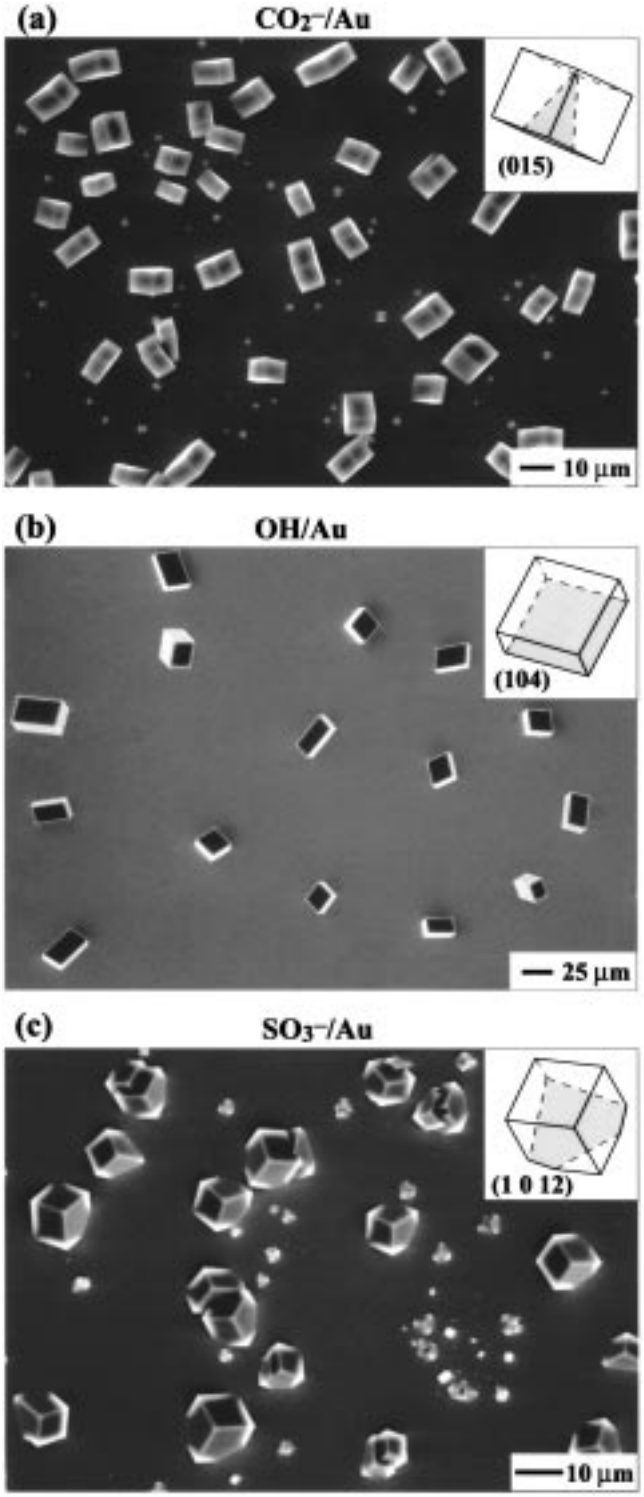

Figure 7. Scanning electron micrographs showing the face-selective nucleation of calcite crystals mediated by SAMs supported on gold: (a) CO_2^-/Au; (b) OH/Au; and (c) SO_3^-/Au. The inserts present computer generated simulations of the regular calcite rhombohedra viewed down perpendicular to the corresponding average nucleating face (shadowed).

respectively (Figure 9a−c). For PO_3^{2-}/Ag, again, the crystals appeared to all nucleate from planes that form the same angle (∼40°) with the *c*-axis (Figure 9d). This angle corresponds well to the angle formed by the C_n−P bond in this monolayer with the surface normal (see Figure 3b). The orientations of calcite crystals were clearly random for the CH_3/Au and bare Ag (Figure 9e,f).

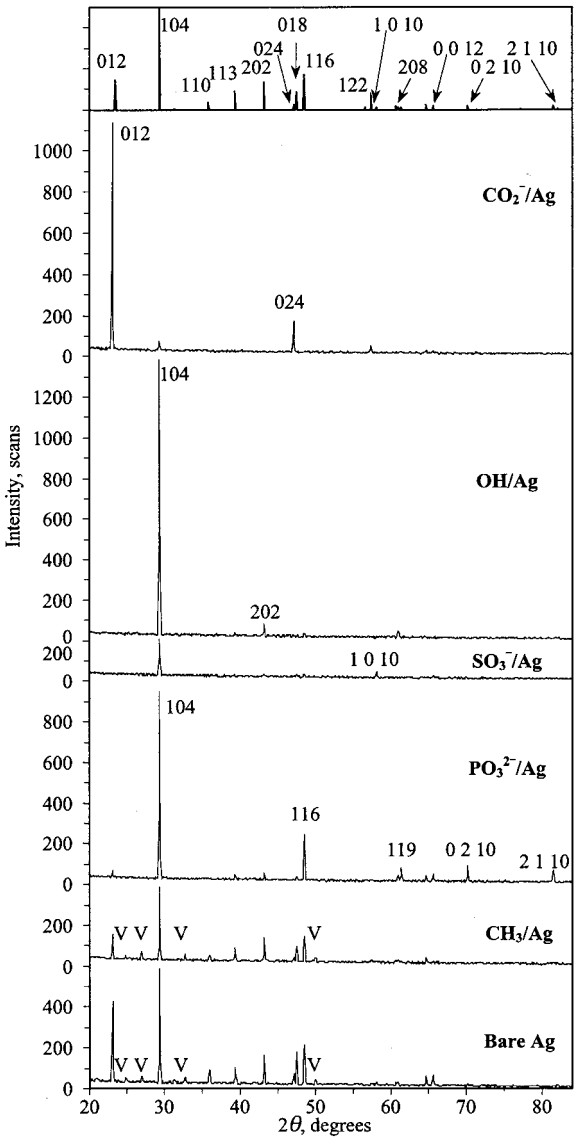

Figure 8. X-ray diffraction data of calcite crystals grown on monolayers of $HS(CH_2)_nX$ supported on silver. Top: A standard diffraction spectrum of the randomly oriented calcite powder.[46] The indices of the crystallographic planes are indicated over the corresponding diffraction lines. Symbol "V" denotes reflections from vaterite.

Figure 10 shows representative SEMs of oriented calcite crystals grown on SAMs supported on Ag and compares them to computer simulations of the (104) calcite rhombohedra nucleated from the corresponding NP_{MA} derived from Figure 9.

Comparison of Crystallization on Different Surfaces. We formed a number of organic surfaces with different chemistry and/or structure of the interfaces involved in controlling nucleation. Table 5 summarizes the results of oriented crystal growth on different surfaces. The CO_2^- -, OH-, and SO_3^- -terminated SAMs supported on silver and gold induced highly oriented nucleation from six different crystallographic planes; PO_3^{2-} -terminated SAMs were selective for planes that form the same angle with the *c*-axis. The angular deviation from the average nucleating planes was 2−5%, conceivably due to the slight differences in the tilt angle in the monolayers[21,22] and/or the roughness of the surface. The percentages of oriented crystals estimated using morphological analysis is clearly higher than the values derived from the XRD spectra, since only a portion of the crystals in each cluster matches precisely the orientations

Table 4. Crystallographic Orientation of Calcite Crystals Grown on SAMs Supported on Silver Estimated from XRD Data

		CO_2^-/Ag		OH/Ag		SO_3^-/Ag		PO_3^{2-}/Ag		CH_3/Ag		bare Ag	
h k l	standard int, I^* [a]	I[b]	%[c]	I[b]	%[c]	I[b]	%[c]	I[b]	%[c]	I[b]	%[c]	I[b]	%
0 1 2	29	100	**81.7**					3	1.6	34	10.7	71	13.8
1 0 4	100	4	0.9	100	**81.1**	100	31.7	100	15.3	100	9.1	100	5.6
1 1 0	7									6	7.8	11	8.8
1 1 3	18			1	4.5			1	0.8	15	7.6	13	4.1
2 0 2	27			4	12.0	3	3.5	2	1.1	29	9.8	23	4.8
0 1 8	17					2	3.7	1	0.9	19	10.2	26	8.6
1 1 6	34			1	2.4	4	3.7	12	5.4	31	8.3	33	5.5
2 1 1	2												
1 2 2	15	3	4.7							2	1.2	1	0.4
1 0 10	2					2	31.7			1	4.6	2	5.6
2 1 4	3									2	6.1	2	3.8
1 1 9	2							3	22.9	1	4.6		
3 0 0	5	1	4.7					2	6.1	6	10.9	8	9.0
0 0 12	3	1	7.9			2	21.2	2	10.2	2	6.1	9	16.9
0 2 10	3							4	20.4			1	1.9
1 1 12	<1												
2 1 10	3							3	15.3	1	3.0		
0 1 14	<1											1	11.3

[a] JCPDS data[46] showing the intensities of peaks in the XRD profile for randomly oriented calcite powder. [b] Measured intensity of peaks in XRD profiles of calcite crystals grown on different surfaces. [c] Percentage of crystals in different orientations estimated using eq 1.

Table 5. Average Nucleation Plane and Percentage of Oriented Calcite Crystals Grown on SAMs Supported on Gold and Silver

	Au					Ag				
				percentage of oriented crystals					percentage of oriented crystals	
SAM	nucleation plane, NP_{MA}[a]	dihedral angle, δ,[b] deg	angular deviation,[c]	from morphological analysis	from XRD analysis	nucleation plane, NP_{MA}[a]	dihedral angle, δ,[b] deg	angular deviation,[c] deg	from morphological analysis	from XRD analysis
CO_2^-	(015)	41	4.3	97	73	(012)	60	3.6	97	82
OH	(104)	43	3.6	100	91	(103)	56	5.1	97	81
SO_3^-	(1 0 12)	21	3.4	78	56	(107)	35	2.7	78	63
PO_3^{2-}	(*hkl*)	24	3.3	95	78[d]	(*hkl*)	40	2.8	95	74[d]

[a] Average nucleation plane NP_{MA} corresponds to the highest density in Figures 6 and 9. [b] Average dihedral angle between the NP_{MA} and (001) plane. [c] Standard angular deviation from the NP_{MA}. [d] A sum of values that correspond to the crystallographic planes within the zone (see Figures 6d and 9d).

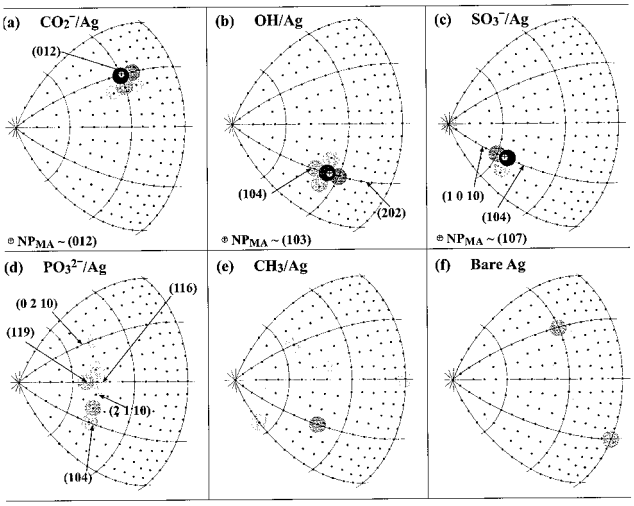

Figure 9. Morphological analysis of orientations of calcite crystals grown on SAMs supported on silver: (a) CO_2^-/Ag; (b) OH/Ag; (c) SO_3^-/Ag; (d) PO_3^{2-}/Ag; (e) CH_3/Ag; and (f) bare Ag. The indices of the crystallographic planes are indicated.

of crystals that contribute to the diffraction pattern (indicated by arrows in Figures 6 and 9).

The fact that the orientation of crystals is uniform for each SAM implies that the specific interfacial structure of the oriented, homogeneous SAM is controlling the orientation of the incipient crystals. To support this conclusion, we analyzed the extent of oriented nucleation as a function of the density of defects in SAMs. The Au films were allowed to soak in the solution of $HS(CH_2)_{15}CO_2H$ for different periods of time (t = 1, 2, 5, 15, and 30 s, 1 and 5 min, 1 and 24 h). The surface of the SAM formed anneals over time, and the number of defects decrease.[38,39,48] Accordingly, the percentage of oriented calcite crystals grown on these SAMs increases (Figure 11); it reaches 100% for t > 1 min.

Although the lattice of the SAMs bearing different functional groups supported on the same metal are similar, these SAMs differ in the character of the interface between the monolayer and crystallizing solution—the structure, chemical character, and coordination number of the terminal groups. Accordingly, these SAMs induced nucleation of calcite from different crystallographic planes. Different orientations of crystals were also observed for SAMs of the same thiol supported on Au and Ag (Table 5); these SAMs have the same exposed terminal functional group, but different geometry (Figure 3). For each pair (X/Au and X/Ag) the angles between the crystallographic orientations of calcite crystals they nucleate is ~15−20°; this number corresponds, we note, to the difference in the tilt of the thiol molecules (α) in the SAMs on Au and Ag (Figure 3).[22] Figure 12a illustrates this relationship using the oriented nucleation of calcite from the (015) and (012) crystallographic planes induced by SAMs of $HS(CH_2)_{15}CO_2H$/Au and $HS(CH_2)_{15}CO_2H$/Ag.

In the case of PO_3^{2-} -terminated SAMs, we can suggest that the driving force for orienting the nuclei is the angle of outward

(48) Zhao, X.-M.; Wilbur, J. L.; Whitesides, G. M. *Langmuir* **1996**, *12*, 3257−3264.

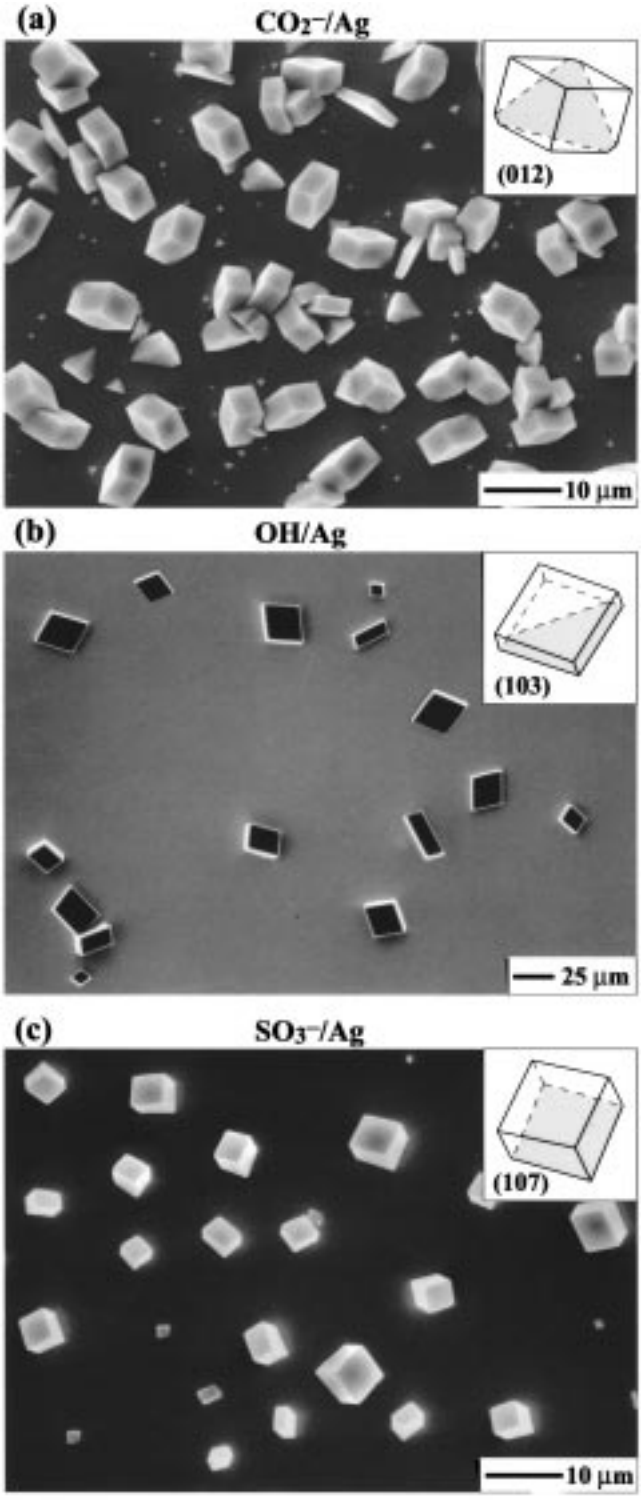

Figure 10. Scanning electron micrographs showing the face-selective nucleation of calcite crystals mediated by SAMs supported on silver: (a) CO_2^-/Ag; (b) OH/Ag; and (c) SO_3^-/Ag. The inserts present the computer-generated simulations of the regular calcite rhombohedra viewed down perpendicular to the corresponding average nucleating face (shadowed).

growth of the calcite *c*-axis directed by the substrate. As a result, nucleation is specific for all the planes that form the same angle with the *c*-axis (Figures 6d and 9d). It is, however, not the case for the CO_2^- -, OH-, and SO_3^- -terminated SAMs that each selectively nucleate calcite from only one crystallographic plane. It is, therefore, conceivable that the observed orientations of crystals are not "apparent" orientations related to their particular

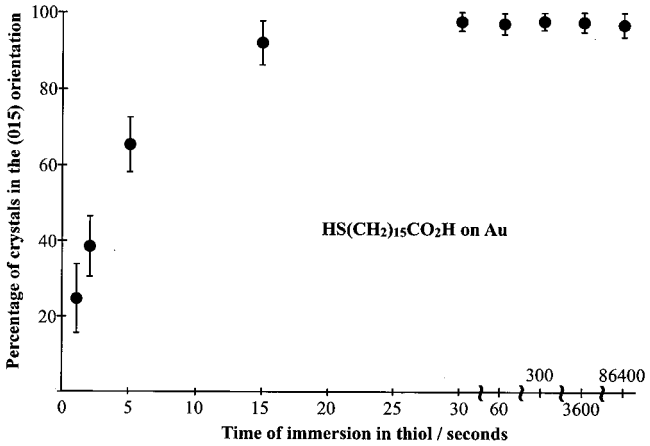

Figure 11. Percentage of oriented calcite crystals nucleated from the (015) plane as a function of the time of the preparation of the SAM of $HS(CH_2)_{15}CO_2H$ on Au.

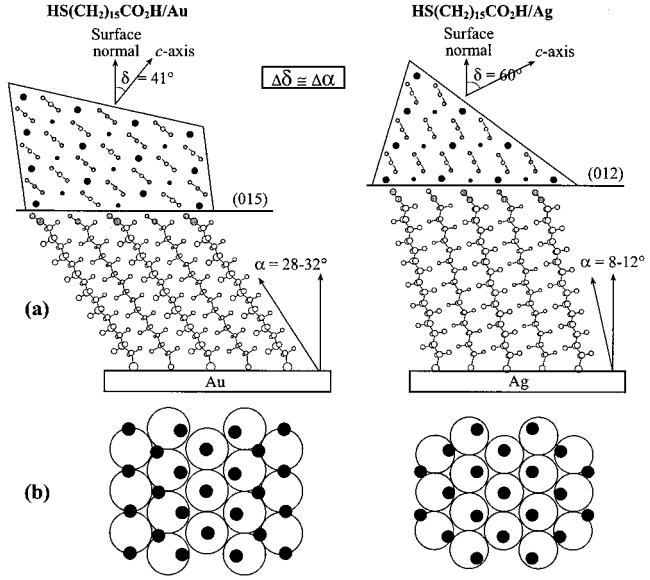

Figure 12. Schematic presentation (to scale) of the geometrical relationship between the structure of the monolayer of $HS(CH_2)_{15}COOH$ supported on gold (left) and silver (right) and the oriented calcite crystal it nucleates. (a) Relative orientations of the SAM and the nucleated crystals. Note the possible coalignment of the carboxylate groups in the SAM and of the carbonates in the nucleated face. (b) Superposition of the lattices of the carboxylate groups in the undistorted SAM (large, open circles) and the Ca^{2+} ions in the nucleated face (small, solid circles).

relationship to the outward growth of the *c*-axis. We believe that the nucleating planes that were observed—two stable crystallographic planes ((104) and (012)) and four "unusual" planes ((015), (1 0 12), (103), and (107))—are the actual nucleating planes stabilized by the substrate. It is important to note that in most cases, we did not observe a satisfactory matching between the lattices of the SAMs and crystal planes they nucleate (Figure 12b), but that there always existed a certain orientation of the functional groups in the SAM that precisely matched the orientation of the carbonate ions in the nucleated crystal (Figure 12a).

Mann and co-workers have studied the oriented nucleation of calcium carbonate under Langmuir monolayers of long-chain alkanes terminated in different functional groups (CO_2H, SO_3H, PO_3H_2, OH). They showed that OH-terminated monolayers had no effect on calcite nucleation; CO_2H-terminated monolayers induced oriented nucleation of the calcite (100) plane; and

SO_3H- and PO_3H_2-terminated monolayers promoted nucleation of the calcite (001) face. The lattice of the close-packed Langmuir monolayers ($a \sim 5$ Å) matches closely that of both the hexagonal (001) plane of calcite ($a = 5$ Å) and the orthorhombic (100) plane of calcite ($a_1 = 5$ Å, $a_2 = 8.5$ Å) (see Figure 2). The authors suggested that matching the symmetry of the functional groups in the monolayer and carbonate anions in the nucleated calcite plane may account for the nucleation from these two planes: the bidentate motif of oxygen atoms in CO_2H-terminated monolayers favors the nucleation of the (100) plane in which carbonate anions are perpendicular to the plane, and the tridentate motif of oxygen atoms in SO_3H- and PO_3H_2-terminated monolayers favors the nucleation of the (001) plane in which carbonate anions are parallel to the plane.

This mechanism alone fails, however, to explain a variety of orientations observed in our work. For example, SAMs supported on gold ($a = 5$ Å) would then be expected to induce nucleation from either the (100) or the (001) plane, depending on the symmetry of the headgroups. Neither of these planes nucleated, and moreover, the SO_3H- and PO_3H_2-terminated SAMs showed different orientational specificity. We believe that the advantage of our work over other studies reporting oriented crystal growth is the ability to induce selective nucleation in a wide variety of orientations. This result provides a basis for more detailed mechanistic studies. Recently, we have been investigating the correlation between the structures of different SAMs of $HS(CH_2)_nCO_2H$/M—with odd and even n[49] and different M (Au(111), Au(100), Ag, Pd, GaAs, Hg, Cu)—and of oriented calcite crystals they nucleate; these results, and general theoretical discussion, will be reported separately. The value of our approach stems from the fact that SAMs provide a system in which the spacing, ordering, and orientation of the *same* terminal group—parameters that cannot be easily controlled on other organic surfaces—can be varied systematically by self-assembly of a common thiol on different surfaces.

Patterned Growth of Calcite in Different Orientations. We have shown[50] that SAMs of alkanethiols on metal substrates can be patterned on the micron scale using microcontact printing. We used this ability to form high-resolution patterns of oriented crystals grown on patterned SAMs terminated in different functional groups (Figure 13). By adjusting the geometry and sizes of the features in the stamp, the concentration of the solution, and the functionality of the surface of the SAM, we could fabricate the arrays of oriented crystals with controlled density of nucleation in defined locations.[51] Figure 13a–c shows examples of calcite crystals grown on gold surfaces bearing different, microprinted SAMs: Figure 13a presents a two-dimensional array of densely nucleated calcite crystals grown from the (015) plane on circular islands of the $HS(CH_2)_{15}CO_2^-$ SAM passivated, in the background, by the $HS(CH_2)_{11}N(CH_3)_3^+$ SAM; Figure 13b shows a square array of discrete calcite crystals nucleated from the (104) plane on the circles of $HS(CH_2)_{11}OH$ in the background of $HS(CH_2)_{15}CH_3$ and illustrates the ability to grow one crystal per nucleating region; Figure 13c shows an example of the localized growth of calcite from two different crystallographic planes—the (015) and (104)—initiated by SAMs composed of alternating strips of $HS(CH_2)_{15}CO_2H$ and $HS(CH_2)_{11}OH$ supported on a gold surface.

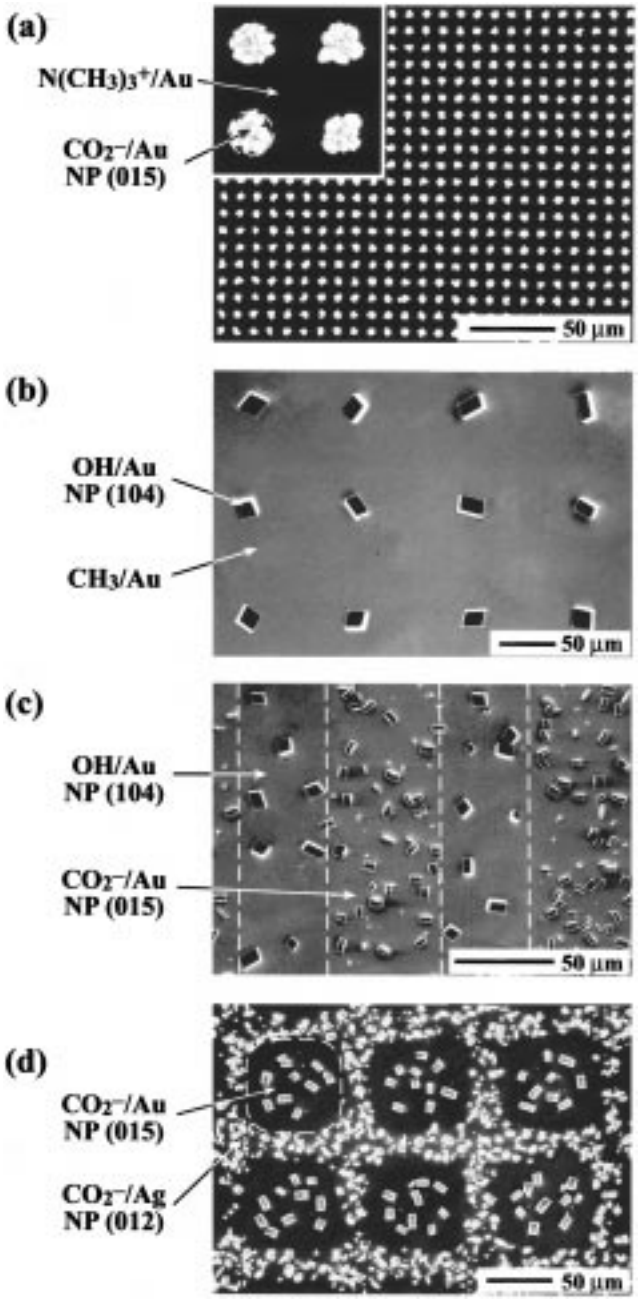

Figure 13. Micropatterns of oriented calcite crystals. The dashed lines outline the geometry of printed regions. (a) A square array of densely nucleated calcite crystals grown from the (015) nucleating plane (NP) on the 4 μm circular islands of $HS(CH_2)_{15}CO_2^-$ in the background of $HS(CH_2)_{11}N(CH_3)_3^+$ supported on a gold surface. (b) A square array of discrete calcite crystals nucleated from the (104) plane on the 50 μm circles of $HS(CH_2)_{11}OH$ in the background of $HS(CH_2)_{15}CH_3$. (c) Lines of calcite crystals nucleated from the (015) and (104) crystallographic planes mediated by SAMs patterned using microcontact printing into alternating 50 μm strips of $HS(CH_2)_{15}CO_2H$ and $HS(CH_2)_{11}OH$ on a gold surface. (d) Islands of calcite crystals nucleated selectively from the (015) plane in the background of calcite crystals nucleated from the (012) plane formed using Ag film micropatterned with Au islands and supporting SAM of $HS(CH_2)_{15}CO_2H$.

This paper shows that oriented nucleation of calcite from different crystallographic planes can occur on SAMs of the *same* thiol supported on *different* metals (Au and Ag). This ability to nucleate selective growth provides an alternative approach to the formation of micropatterns of oriented crystals using substrates micropatterned with regions of Au and Ag supporting SAMs.[52] Figure 13d presents an example of the micropatterned

(49) Popovitz-Biro, R.; Wang, J. L.; Majewski, J.; Shavit, E.; Leiserowitz, L.; Lahav, M. *J. Am. Chem. Soc.* **1994**, *116*, 1179–1191.
(50) Kumar, A.; Abbott, N. L.; Kim, E.; Biebuyck, H. A.; Whitesides, G. M. *Acc. Chem. Res.* **1995**, *28*, 219–226.
(51) Aizenberg, J.; Black, A. J.; Whitesides, G. M. *Nature* **1999**, *398*, 495–498.

growth of calcite from the (015) and (012) planes on a SAM of $HS(CH_2)_{15}CO_2H$ supported on a Ag film patterned with Au islands.

Conclusions

The use of functionalized alkanethiols self-assembled on metal surfaces as substrates for crystallization of calcite makes it possible to achieve a high level of control over crystal orientations. Our data imply that face-selective crystallization of calcite is substantially controlled by the geometry of the array of certain terminal functional groups (CO_2^-, SO_3^-, and OH) at the interface between the SAM and the solution.

Using this approach, we achieved selective nucleation of calcite from six crystallographic planes—(015), (104), (1 0 12), (012), (103), and (107). To the best of our knowledge, this is the first time that calcite crystals have been grown in such a variety of orientations in an artificially controlled system. The use of Langmuir monolayers and of adsorbed biological macromolecules as organic substrates for oriented nucleation has resulted only in calcite growth from the (100) and (001) faces.[4,13,15,30] Calcite growth from the (012) plane has been reported for the surface of acidic polydiacetylene films.[17] The selectivity of these crystallization processes was lower than in the method proposed in our work, presumably due to the more ordered structure of SAMs formed on metals compared to that of Langmuir monolayers and of adsorbed macromolecules.

The ability to pattern SAMs of alkanethiols on metal substrates on a micron scale is another important property of these organic surfaces. Using this ability, for the first time, we formed high-resolution patterns of differently oriented crystals.

The design of various interfacial structures by self-assembly of alkanethiols on different supports is, therefore, a promising approach to the control of the formation of oriented crystals and to the study of the mechanisms of the oriented nucleation.

Experimental Section

Substrates. Silicon wafers (Silicon Sense, test grade, n or p type) were coated with 2 nm of Ti, to promote adhesion, and then typically with 50 nm of metal (Ag or Au) using an electron beam evaporator (base pressure 10^{-7} Torr).

SAMs. SAMs of $HS(CH_2)_{15}CO_2H$, $HS(CH_2)_{11}OH$, $HS(CH_2)_{11}SO_3H$, $HS(CH_2)_{11}PO_3H_2$, $HS(CH_2)_{11}N(CH_3)_3Cl$, and $HS(CH_2)_{15}CH_3$ were formed on metal substrates by exposing the surfaces to a 10 mM solution of the thiol in ethanol for 24 h, followed by washing with ethanol.[38] The quality of SAMs was characterized using contact angle measurements; the angles corresponded well to those reported in ref 20. Patterned SAMs on Au were formed using microcontact printing:[50] PDMS stamps with different relief structures—square array of 4 μm circles separated by 6 μm spaces (Figure 13a), square array of 50 μm circles separated by 50 μm spaces (Figure 13b), and 50 μm lines separated by 50 μm spaces (Figure 13c)—"inked" with a 10 mM solution of $HS(CH_2)_{15}CO_2H$ (Figure 13a) and $HS(CH_2)_{11}OH$ (Figure 13b,c) in ethanol and brought into conformal contact with gold for 10 s; the noncontact areas were then derivatized with a 10 mM solution of $HS(CH_2)_{11}N(CH_3)_3Cl$ (Figure 13a), $HS(CH_2)_{15}CH_3$ (Figure 10b), and $HS(CH_2)_{15}CO_2H$ (Figure 10c) in ethanol by immersion for 1 min. Patterned SAMs were also formed on silicon wafers patterned with microregions of Ag and Au (Figure 13d) by depositing Au (50 nm) through a stencil (a TEM grid) on a Ag film (50 nm) and then immersing the surfaces in a 10 mM solution of $HS(CH_2)_{15}CO_2H$ in ethanol.[52]

Crystallization. The substrates were placed upside-down on supports (5 mm high) in 10 mM calcium chloride solution in a closed desiccator containing vials of ammonium carbonate.[15,31,35] To minimize contamination of SAMs, the substrates were usually placed into calcium chloride solution immediately after the exposure to the solution of thiol. All experiments were carried out at room temperature for 1 h. Precipitation of calcium carbonate results from the diffusion of carbon dioxide vapor into the $CaCl_2$ solution, according to the following reactions:

$$(NH_4)_2CO_3(s) \rightarrow 2NH_3(g) + CO_2(g) + H_2O$$

$$CO_2 + Ca^{2+} + H_2O \rightarrow CaCO_3(s) + 2H^+$$

$$2NH_3 + 2H^+ \rightarrow 2NH_4^+$$

The use of $(NH_4)_2CO_3$ rather than carbon dioxide allowed us to maintain neutral pH in the crystallization solution.

Analysis. The crystals, once formed, were examined using optical microscopy to determine the densities of nucleation and crystal sizes. The specific crystallographic orientations of the crystals relative to the interface between the SAM and the solution were analyzed using XRD in the $\theta-2\theta$ scan mode. In this mode, only diffracting planes parallel to the plane of the substrate (nucleating planes) produce significant diffraction intensity. The peaks present in the XRD profile represent, therefore, the predominant crystallographic orientations of the crystals.

A detailed morphological analysis was undertaken to confirm the assignment of each specific crystallographic orientation and to estimate the deviation in angle of the crystals from these directions of growth. A population of 40 crystals was used in statistics for each surface type. The crystals were viewed down the surface normal in a scanning electron microscope (JEOL 6400) (SEM). We measured the three angles (α, β, γ) between the crystal edges meeting at the upper corner of the crystal (Figure 2a). The nucleation plane was assigned using known structural relationships in the calcite unit cell[26,28] that unequivocally relate the orientation of the regular {104} calcite rhombohedra vis-à-vis the interface to the measured angles and the symmetry of truncations with the substrates.

Acknowledgment. This work was partially supported by MURI/ARD under grant DAAH 0495-1-0102 and used MRSEC Shared Facilities supported by the NSF under award number DMR-9400396.

JA984254K

(52) Aizenberg, J.; Black, A. J.; Whitesides, G. M. *Nature* **1998**, *394*, 868−871.